Partial differential equations and variational methods for geometric processing of images

Buet, Blanche; Mirebeau, Jean-Marie; van Gennip, Yves; Desquilbet, François; Dreo, Johann; Leonardi, Gian Paolo; Masnou, Simon; Schönlieb, Carola-Bibian

Publication date
2019

Document Version
Final published version

Published in
Journal of Computational Mathematics

SMAI-JCM
SMAI Journal of Computational Mathematics

Partial differential equations and variational methods for geometric processing of images

Blanche Buet, Jean-Marie Mirebeau, Yves van Gennip, François Desquilbet, Johann Dreo, Frédéric Barbaresco, Gian Paolo Leonardi, Simon Masnou & Carola-Bibiane Schönlieb

Volume S5 (2019), p. 109-128.

<http://smai-jcm.centre-mersenne.org/item?id=SMAI-JCM_2019__S5__109_0>

Publication membre du
Centre Mersenne pour l'édition scientifique ouverte
http://www.centre-mersenne.org/

Sousmission sur https://smai-jcm.math.cnrs.fr/index.php/SMAI-JCM

SMAI Journal of Computational Mathematics
Vol. S5, 109-128 (2019)

Partial differential equations and variational methods for geometric processing of images

Blanche Buet [1]
Jean-Marie Mirebeau [2]
Yves van Gennip [3]
François Desquilbet [4]
Johann Dreo [5]
Frédéric Barbaresco [6]
Gian Paolo Leonardi [7]
Simon Masnou [8]
Carola-Bibiane Schönlieb [9]

[1] Laboratoire de Mathématiques d'Orsay, Univ. Paris-Sud, CNRS, Université Paris-Saclay, 91405 Orsay, France
E-mail address: blanche.buet@u-psud.fr
[2] Laboratoire de Mathématiques d'Orsay, Univ. Paris-Sud, CNRS, Université Paris-Saclay, 91405 Orsay, France
E-mail address: jean-marie.mirebeau@math.u-psud.fr
[3] DIAM, Technical University of Delft, Netherlands
E-mail address: Y.vanGennip@tudelft.nl
[4] École Normale Supérieure de Paris, France
E-mail address: francois.desquilbet@ens.fr
[5] Thales Research and Technology, France
E-mail address: johann.dreo@thalesgroup.com
[6] Thales Land & Air Systems, France
E-mail address: frederic.barbaresco@thalesgroup.com
[7] Dipartimento di Matematica, Università di Trento, Italy
E-mail address: gianpaolo.leonardi@unitn.it
[8] Univ Lyon, Université Claude Bernard Lyon 1, CNRS UMR 5208, Institut Camille Jordan, F-69622 Villeurbanne, France
E-mail address: masnou@math.univ-lyon1.fr
[9] DAMTP, University of Cambridge, United Kingdom
E-mail address: cbs31@cam.ac.uk.

Introduction (by S. Masnou and C.-B. Schönlieb)

This paper arose from a minisymposium held in 2018 at the 9th International Conference on Curves and Surface in Arcachon, France, and organized by Simon Masnou and Carola-Bibiane Schönlieb. This

BB was supported by a PEPS JCJC grant from CNRS, JMM acknowledges support by French National Research Agency research grant MAGA, ANR-16-CE40-0014.
SM acknowledges support from the French National Research Agency (ANR) research grant MIRIAM (ANR-14-CE27-0019) and the European Union Horizon 2020 research and innovation programme under the Marie Skodowska-Curie grant agreement No 777826 (NoMADS).
CBS acknowledges support from the Leverhulme Trust project on Breaking the non-convexity barrier, the Philip Leverhulme Prize, the EPSRC grant Nr. EP/M00483X/1, the EPSRC Centre Nr. EP/N014588/1, the European Union Horizon 2020 research and innovation programmes under the Marie Skodowska-Curie grant agreement No 777826 NoMADS and No 691070 CHiPS, the Cantab Capital Institute for the Mathematics of Information and the Alan Turing Institute.

minisymposium featured a variety of recent developments of geometric partial differential equations and variational models which are directly or indirectly related to several problems in image and data processing. The current paper gathers three contributions which are in connection with the talks of three minisymposium speakers: Blanche Buet, Jean-Marie Mirebeau, and Yves van Gennip. The first contribution (Section 1) by Yves van Gennip provides a short overview of recent activity in the field of PDEs on graphs, without aiming to be exhaustive. The main focus is on techniques related to the graph Ginzburg–Landau variational model, but some other research in the field is also mentioned at the end of the section. The second contribution (Section 2), written by Jean-Marie Mirebeau, François Desquilbet, Johann Dreo, and Frédéric Barbaresco presents a recent numerical method devoted to computing curves that globally minimize an energy featuring both a data driven term, and a second order curvature penalizing term. Applications to image segmentation are discussed, and recent progress on radar network configuration, in which the optimal curves represent an opponent's trajectories, is described in detail. Lastly, Section 3 is devoted to a work by Blanche Buet, Gian Paolo Leonardi, and Simon Masnou on the definition and the approximation of weak curvatures for a large class of generalized surfaces, and in particular for point clouds, based on the geometric measure theoretic notion of varifolds.

1. PDEs and variational models on graphs (by Y. van Gennip)

Partial differential equations (PDEs) are equations that contain the partial derivatives of multivariate functions. They are widely used in the modelling of phenoma in physics, economics, biology, and other sciences. The field of PDEs on graphs deals with discretisations of PDEs on graphs (networks), which then take the form of coupled ordinary differential equations (ODEs) or difference equations. Contrary to numerical analysis, which typically deals with discretisations of PDEs on regular grids, the area of PDEs on graphs is often interested in networks with highly irregular structures. Moreover, where numerical analysis usually aims to minimize the effect which the structure of the discretisation has on the outcome of the numerical scheme (because its goal is to approximate the solution to a continuum PDE), in the world of PDEs on graphs the graph structure tends to carry important information about the underlying application which needs to be preserved. Apart from the new theoretical challenges which such discretised equations pose, applications in the imaging and data sciences are strong motivators which have driven a rapid growth in research in this area in recent years.

In this section we will give a short overview of recent activity in the field of PDEs on graphs, without aiming to be exhaustive. The main focus will be on techniques related to the graph Ginzburg–Landau variational model. At the end of this section we will briefly touch on some other research in the field.

1.1. The Ginzburg–Landau variational model

As a convenient starting point for our overview we use the 2012 paper by Andrea Bertozzi and Arjuna Flenner [8] in which the authors explicitly translate a well-known continuum variational model to the graph setting, reminiscent of the nonlocal approaches in papers such as [13, 44]. The calculus of variations deals with models posed in the form of a minimization (or maximization) problem. Typically this minimization is of a functional over a function space; such variational models are closely related to differential equations: The Euler–Lagrange equations associated with the minimization problem take the form of ordinary or partial differential equations. Also gradient flows, which are used to find (local) minimizers are usually PDEs. In [8] the authors proposed a graph version of the Ginzburg–Landau functional to address image segmentation, graph clustering, and classification problems. The classic Ginzburg–Landau functional,

$$F(u) := \varepsilon \int_\Omega |\nabla u|^2 \,\mathrm{d}x + \frac{1}{\varepsilon} \int_\Omega W(u) \,\mathrm{d}x,$$

is a variational model for phase separation. Minimizers $u : \Omega \to \mathbb{R}$ of F are forced, through minimization of the double well term $\frac{1}{\varepsilon}\int_\Omega W(u)\,\mathrm{d}x$ (for small, positive, ε) to attain values close to the minima of $W(u) = u^2(1-u)^2$. Hence the domain Ω will be divided into two phases: $\{u \approx 0\}$ and $\{u \approx 1\}$. The gradient term $\varepsilon\int_\Omega |\nabla u|^2\,\mathrm{d}x$ on the other hand, penalises surface area between the two phases. Minimization of the functional F is usually considered under a fixed mass constraint of the form $\int_\Omega u\,\mathrm{d}x = M$, which is natural in the material sciences context in which this model originated.

In [8] the graph functional

$$f(u) := \sum_{i,j\in V} \omega_{ij}(u_i - u_j)^2 + \frac{1}{\varepsilon}\sum_{i\in V} W(u_i)$$

was introduced, which is the graph analogue of F. Now the functions $u : V \to \mathbb{R}$ have the vertex set V of a given finite, simple, undirected graph as domain. The term $\sum_{i,j\in V}\omega_{ij}(u_i-u_j)^2$ (where ω_{ij} is a nonnegative weight on the edge between nodes i and j and u_i is the value of the function u on node i) plays a role similar to the gradient term in F: When ω_{ij} is large, minimization of f leads u to have similar values at nodes i and j. The double well potential term $\frac{1}{\varepsilon}\sum_{i\in V} W(u_i)$, as before, serves to force u to take values close to 0 or 1.

Minimization of the functional f therefore gives a labelling function u which assigns values approximately equal to 0 or 1 to the vertices in such a way that vertices connected by a highly weighted edge have similar values. This functional can be combined with either a mass constraint or an additional data fidelity term of the form $\sum_{i:\text{ training data}}(u_i - u_i^{\text{training}})^2$ to cluster or classify the nodes of a graph into two groups ("phases" where $u \approx 0$ and $u \approx 1$) based on the pairwise node similarity encoded in the edge weights ω_{ij}. By treating the pixels of an image as nodes in a graph, data classification can be used for image segmentation as well.

1.2. **PDEs on graphs as nonlinear relaxations of NP hard problems**

The problem of finding a balanced clustering, i.e. a clustering whose clusters have approximately similar sizes, is known to be NP hard [84, 85]. The variational Ginzburg–Landau method above can be seen as a nonlinear relaxation which approximates this NP hard problem. This connection can be seen especially clearly if we consider the gradient flow equation associated with f, the graph Allen–Cahn equation:

$$\frac{\mathrm{d}u_i}{\mathrm{d}t} = -\sum_{j\in V}\omega_{ij}(u_i - u_j) - \frac{1}{\varepsilon}W'(u_i) + c(u).$$

Here $c(u)$ is the term coming from the mass constraint or data fidelity term; for simplicity of the discussion, we will assume c is absent in what follows. By recognising $(\Delta u)_i := \sum_{j\in V}\omega_{ij}(u_i - u_j)$ as the combinatorial graph Laplacian from spectral graph theory [24, 84], we see that this nonlinear gradient flow equation is closely connected with spectral clustering [84]. This connection is also present in another often used method for approximately minimising f, a graph version of the threshold dynamics (or Merriman–Bence–Osher; MBO) scheme [62]:

$$u_i^{k+1} = \begin{cases} 0, & \text{if } \tilde{u}_i(\tau) < \frac{1}{2}, \\ 1, & \text{if } \tilde{u}_i(\tau) \geq \frac{1}{2}, \end{cases} \quad \text{where } \tilde{u}(t) \text{ solves } \begin{cases} \frac{\mathrm{d}\tilde{u}_i}{\mathrm{d}t} = -\sum_{j\in V}\omega_{ij}(\tilde{u}_i - \tilde{u}_j), \\ \tilde{u}(0) = 0. \end{cases}$$

The parameter $\tau > 0$ determines the length of the graph diffusion process, before thresholding happens. In practice, these equations can be solved quickly and accurately, although there are as of yet no theoretical guarantees on the accuracy [8, 56, 61]. Using techniques such as truncated spectral decomposition of the graph Laplacian and convex splitting, allow these methods to be scaled to very large graphs, while matrix completion techniques such as the Nyström extension [36, 68] and fast eigenvalue

computation algorithms such as the Rayleigh–Chebychev algorithm [3] make the construction of such large graphs feasible in the first place.

The graph Ginzburg–Landau technique has been used successfully in, for example, data clustering and classification and image segmentation [8, 19, 61] and has also been extended to deal with clustering and classification into more than two classes [37, 38, 39, 59, 60]. Figure 1.1 shows an example of an image segmentation result from [19].

Figure 1.1. Image segmentation result from [19].

The success of the Ginzburg–Landau clustering technique to approximate the NP hard balanced clustering problem suggests that other similarly hard combinatorial problems might be approachable using these techniques. In [52] the solution to the max-cut problem (i.e. partition the node set of a graph into two sets such that the cut between them is maximal) is approximated by minimizers of the graph functional

$$f^+(u) := \sum_{i,j\in V} \omega_{ij}(u_i + u_j)^2 + \frac{1}{\varepsilon}\sum_{i\in V} W(u_i).$$

A generalisation to the k-colouring problem is given in [51]. By again deriving an Allen–Cahn like equation or MBO type scheme from f^+ (or its multi-phase generalisation), which uses the *signless* graph Laplacian, fast scalable methods for finding maximum cuts or k-colourings are obtained. Combining regular and signless graph Laplacians also allows for clustering of signed networks, i.e. networks with both positively and negatively weighted edges [26].

1.3. Connections between the graph Allen–Cahn equation, graph MBO scheme, and graph mean curvature flow

Heuristically the graph MBO scheme described above can be understood as an approximation to the graph Allen–Cahn equation: The nonlinear effect of the term $\frac{1}{\varepsilon}W'(u_i)$, namely driving the solutions u_i to take values in or close to $\{0, 1\}$, is mimicked by the thresholding step in the MBO scheme. In fact, the original continuum Allen–Cahn equation and continuum MBO scheme, which served as inspiration for the graph variants, are closely linked through a third set of dynamics: mean curvature flow (MCF). MCF is the evolution of the boundary of a set with a normal velocity proportional to the local mean curvature of its boundary. It is known that continuum MCF describes the limiting dynamics of continuum Allen–Cahn (as $\varepsilon \to 0$) and of continuum MBO (as $\tau \to 0$) [6, 7, 12, 14, 35].

A natural question to ask is whether there exist similar connections between the graph versions of these dynamics. In [83] graph curvature was introduced, as well as graph MCF based on the continuum variational formulation of MCF in [2, 55, 77]; connections to graph Allen–Cahn and graph MBO are

under investigation, but remain elusive. Recent work, however, shows a direct connection between graph Allen–Cahn and graph MBO [16]: If the double obstacle potential

$$W^{\mathrm{obs}}(x) := \begin{cases} \frac{1}{2}x(1-x), & \text{if } 0 \le x \le 1, \\ +\infty, & \text{otherwise,} \end{cases}$$

is used in the graph Allen–Cahn equation (as for example in [10]), instead of the smooth potential W introduced above, and if $\lambda := \tau/\varepsilon = 1$, then the graph MBO scheme is equivalent to the following implicit Euler semi-discretisation of the Allen–Cahn equation:

$$u^{k+1} = e^{-\tau\Delta}u^k - \frac{\tau}{\varepsilon}W^{\mathrm{obj}'} \circ u^{k+1}.$$

The derivative $W^{\mathrm{obj}'}$ of the non-smooth potential is to be interpreted in the sense of subdifferential calculus. Allowing for values $\lambda \in (0,1)$ provides a natural family of dynamics interpolating between graph diffusion and the MBO scheme.

1.4. **Variational techniques**

Connections between these different graph-based dynamics can also be seen at a variational level, using Γ-convergence techniques. Γ-convergence [11, 27] is a very useful tool for variational problems, since Γ-convergence of the functionals guarantees convergence of minimizers. In [82] it was shown that f Γ-converges to the graph cut objective functional $\sum_{i,j\in V}\omega_{ij}|u_i - u_j|$ ($u_i \in \{0,1\}$ for all i) as $\varepsilon \to 0$. This limit functional can also be interpreted as a graph based total variation, since it is a measure for the interface between the phases $\{u = 0\}$ and $\{u = 1\}$. Hence this Γ-convergence result is seen to be the graph equivalent of a well-known continuum result from [66, 67].

In [83] a Lyapunov functional for the graph MBO scheme was formulated, i.e. a functional whose value decreases along iterates of the MBO scheme (and moreover whose linearisation is minimized by these iterates); subsequently [81] showed that in the limit $\tau \to 0$ (where τ is the diffusion time in the MBO scheme) these Lyapunov functionals also Γ-converge to the graph cut objective functional.

The same paper [81] also introduced a mass conserving MBO scheme in which the thresholding of $\tilde{u}$ to u^{k+1} is not based on the $\frac{1}{2}$-level set, but rather uses an adaptive threshold which guarantees conservation of mass. In [15] the semi-discrete implicit Euler scheme from [16] is used to show that this mass conserving MBO scheme is follows naturally from the mass conserving Allen–Cahn equation.

1.5. **Discrete-to-continuum limits**

The variational setup of these models is not only useful in discovering connections between the different graph-based dynamics, but also allows for a natural discrete-to-continuum limit in terms of Γ-convergence on graphs for which a reasonable continuum limit can be defined. For example, on 4-regular graphs obtained by ever finer discretisations of the flat torus [82] shows that the continuum limit of f is given by an anisotropic total variation which preserves the directionality of the grid, while on point clouds obtained by sampling ever more points from an underlying subset of $\mathbb{R}^n$ a series of papers [42, 43, 78] has shown continuum limits for both the graph based Ginzburg–Landau and total variation functionals. In the latter context these limit results can be interpreted as consistency results that show that the discrete model defined on the samples is asymptotically consistent with a continuum model. The techniques developed to associate point cloud based functions with continuum functions have recently also been applied to prove consistency of other statistical methods [40, 41] and to show that certain artificial neural networks have continuum limits that take the form of ODE-constrained variational models [79]. For discrete-to-continuum limit results, also graphon methods have been considered [45, 46, 58]

1.6. **Further applications**

The above has been only a short, highly incomplete, overview of the rapidly growing field of PDEs on graphs, using the variational Ginzburg–Landau method as starting point. We have not aimed to be exhaustive. Other PDE operators on graphs have found applications in image analysis, such as the p-Laplacian [21, 32, 33, 34, 54, 74, 80]. Other theoretical investigations include [57] and recently these methods have been used to study artificial neural networks [69, 79]. Recent papers have studied consistency and error bounds for semi-supervised learning methods and their dependence on the amount of a priori known data [20, 22, 31, 71].

2. **Generalized fast marching method for computing highest threatening trajectories with curvature constraints and detection ambiguities in distance and radial speed (by J. M. Mirebeau, F. Desquilbet, J. Dreo, and F. Barbaresco)**

2.1. **Globally optimal paths with a curvature penalty**

This section is concerned with planar paths minimizing certain energy functionals, between two given points and with prescribed tangents at these points. The path energy model features a low order data-driven term, and a higher order regularization term. A globally optimal path is found, using optimal control techniques, which involve numerically solving a PDE on the configuration space of positions and orientations. We discuss applications to image segmentation, and motion planning in Section 2.2.

Path energy models. In the models of interest to us, the cost of a smooth planar path $\mathbf{x} : [0, T] \to \Omega$, parametrized by Euclidean arc length and within a domain $\Omega \subset \mathbb{R}^2$, takes the following form:

$$\mathfrak{C}(\mathbf{x}) := \int_0^T \alpha(\mathbf{x}(s), \dot{\mathbf{x}}(s))\, \mathcal{C}(\|\ddot{\mathbf{x}}(s)\|)\, \mathrm{d}s. \tag{2.1}$$

We denoted by $\alpha : \overline{\Omega} \times \mathbb{S}^1 \to]0, \infty[$ an arbitrary continuous data-driven term, depending on the path position and direction. The path local curvature $\kappa = \|\ddot{\mathbf{x}}(t)\|$ (recall that $\|\dot{\mathbf{x}}(s)\| \equiv 1$) is penalized in (2.1) by a cost function $\mathcal{C}(\kappa)$, which may be chosen among the following classical models, here sorted by increasing stiffness:

$$\text{Reeds–Shepp: } \sqrt{1+\kappa^2}, \qquad \text{Euler–Mumford: } 1+\kappa^2, \qquad \text{Dubins: } \begin{cases} 1 & \kappa \leq 1, \\ \infty & \text{else.} \end{cases} \tag{2.2}$$

They are respectively representative of (i) a wheelchair-like robot, (ii) the bending energy of an elastic bar, and (iii) a vehicle with a bounded turning radius. In the case of the Reeds–Shepp model, one must further distinguish between the classical model with reverse gear, and the forward only variant [30].

Viscosity solutions, and the Fast marching algorithm. Data-driven path energies, subject to e.g. fixed endpoints, usually possess many local minima. In order to guarantee that the global minimum is found, path energy minimization must be reformulated as an optimal control problem. The corresponding value function is the unique viscosity solution to a PDE of eikonal type, and the optimal paths can be extracted by backtracking once it is numerically computed [70].

Only simple first order energies, such as $\int_0^T \alpha(\mathbf{x}(s))\|\dot{\mathbf{x}}(s)\|\mathrm{d}s$ could originally be addressed in the viscosity solution framework, typically using the Fast Marching Method (FMM) which solves the eikonal PDE in a single pass over the domain [25]. Recent progress [23, 30, 63] enabled the extension to (2.1) of the FMM. For that purpose the path is lifted in the configuration space of positions and orientations, defining $\gamma(t) = (\mathbf{x}(t), \theta(t))$ subject to the constraint $\dot{\mathbf{x}}(t) = \mathbf{n}(\theta(t))$ where $\mathbf{n}(\theta) := (\cos\theta, \sin\theta)$. This non-holonomic constraint allows to reformulate (2.1) as a first order energy, since

$|\ddot{\mathbf{x}}(t)| = |\dot{\theta}(t)|$. The energy of a non-admissible path $\gamma = (\mathbf{x}, \theta) : [0,1] \to \mathbb{R}^2 \times \mathbb{S}^1$, defined in the augmented space but such that $\dot{\mathbf{x}}(t)$ is not positively proportional to $\mathbf{n}(\theta(t))$ for some $t \in [0,1]$, is defined as $+\infty$, see [63] for details and comparison with alternative approaches such as [53, 75].

For interested readers, we now provide some additional details on the theoretical and numerical approach. Denote by $u(\mathbf{x}, \theta)$ the minimal cost (2.1) of a path from the domain boundary $\partial\Omega$ to the endpoint $\mathbf{x}$ with final tangent $(\cos\theta, \sin\theta)$. Then u, known as the value function to the optimal control problem, is a (possibly discontinuous) viscosity solution [5, 63] to the Bellman equation

$$\mathcal{F}^*_{(\mathbf{x},\theta)}(\nabla u(\mathbf{x},\theta)) = \alpha(\mathbf{x},\theta) \quad \text{in } \Omega \times \mathbb{S}^1, \qquad\qquad u(\mathbf{x},\theta) = 0 \quad \text{on } \partial\Omega \times \mathbb{S}^1,$$

where the α is the data-driven term appearing in (2.1). The Hamiltonian $\mathcal{F}^*$ in the l.h.s. has the following expression: denoting $\hat{x} := \langle \nabla_{\mathbf{x}} u(\mathbf{p}), \mathbf{n}(\theta)\rangle$ and $\hat{\theta} := \partial_\theta u(\mathbf{p})$

$$\text{Reeds–Shepp: } \sqrt{\hat{x}_+^2 + \hat{\theta}^2}, \qquad \text{Euler–Mumford: } \hat{x} + \sqrt{\hat{x}^2 + \hat{\theta}^2}, \qquad \text{Dubins: } \max\{0,\, \hat{x} + \hat{\theta},\, \hat{x} - \hat{\theta}\}.$$

These expressions are derived from the curvature dependent cost $\mathcal{C}$ (2.2) as $\sup\{(\hat{x} + \hat{\theta}\kappa)/\mathcal{C}(\kappa);\, \kappa \in \mathbb{R}\}$. Using adequate techniques, we approximate this Hamiltonian in the following generic form

$$\mathcal{F}^*_{(\mathbf{x},\theta)}(\nabla u(\mathbf{x},\theta))^2 \approx \max_{1\le k\le K} \left(\sum_{1\le i\le I} \alpha_{ik}(\theta) \langle \nabla u(\mathbf{x},\theta), \mathbf{e}_{ik}(\theta)\rangle^2 + \sum_{1\le j\le J} \beta_{jk}(\theta) \max\{0, \langle \nabla u(\mathbf{x},\theta), \mathbf{f}_{jk}(\theta)\rangle\}^2 \right), \quad (2.3)$$

where the weights α_{ik}, β_{jk}, are *non-negative*, and the offsets $\mathbf{e}_{ik}, \mathbf{f}_{jk}$ have *integer* coordinates. The directional derivatives are then approximated using upwind finite differences as in (2.4) below, and the coupled system of equations resulting from the discretized PDE is solved in a single pass over the domain [65]. It would be too long to describe here the approximation procedure [63, 65] yielding (2.3), which involves a relaxation parameter $\varepsilon > 0$ and techniques from algorithmic geometry. Nevertheless let us mention the meta parameters (I, J, K) used: Reeds–Shepp $(1, 3, 1)$, Euler–Mumford $(0, 27, 1)$, Dubins $(0, 6, 2)$. For comparison, the standard d-dimensional isotropic fast marching method [70] can be framed in a similar setting, with $(I, J, K) = (d, 0, 1)$: denoting by $(\mathbf{e}_i)_{i=1}^d$ the canonical basis of $\mathbb{R}^d$

$$\|\nabla u(\mathbf{x})\|^2 = \sum_{1\le i\le d} \langle \nabla u(x), \mathbf{e}_i\rangle^2 \approx \sum_{1\le i\le d} \max\left\{0, \frac{u(\mathbf{x}) - u(\mathbf{x} - h\mathbf{e}_i)}{h}, \frac{u(\mathbf{x}) - u(\mathbf{x} + h\mathbf{e}_i)}{h}\right\}^2. \quad (2.4)$$

Applications to image processing. Image segmentation methods based on active contours typically involve path energies balancing low-order data-driven terms, and higher order regularization terms. Unfortunately, many second order models can only be locally optimized [50], resulting in spurious local minima and high sensitivity to initialization. In contrast, first order models [25] can be globally optimized using the FMM, but the lack of smoothness penalization gives way to various artefacts referred to as leaks, shortcuts, and branches combination problems [23].

Our numerical method combines the best of the two worlds: a second order energy model (2.1), and fast global minimization, with prescribed endpoint positions and tangents. This enables new developments, see for instance [23] on the retina vessel tree segmentation, and [30] on white matter fiber path extraction.

2.2. **Threatening trajectories and radar network configuration**

In a collaboration work with the company Thales, we optimize the configuration of a radar network for protecting an objective within a region, against an enemy assumed to have unlimited intelligence and computing power, and yet whose vehicle is subject to some manoeuverability constraints. The goal is to maximize the probability of detection of the most dangerous trajectory between a given source and

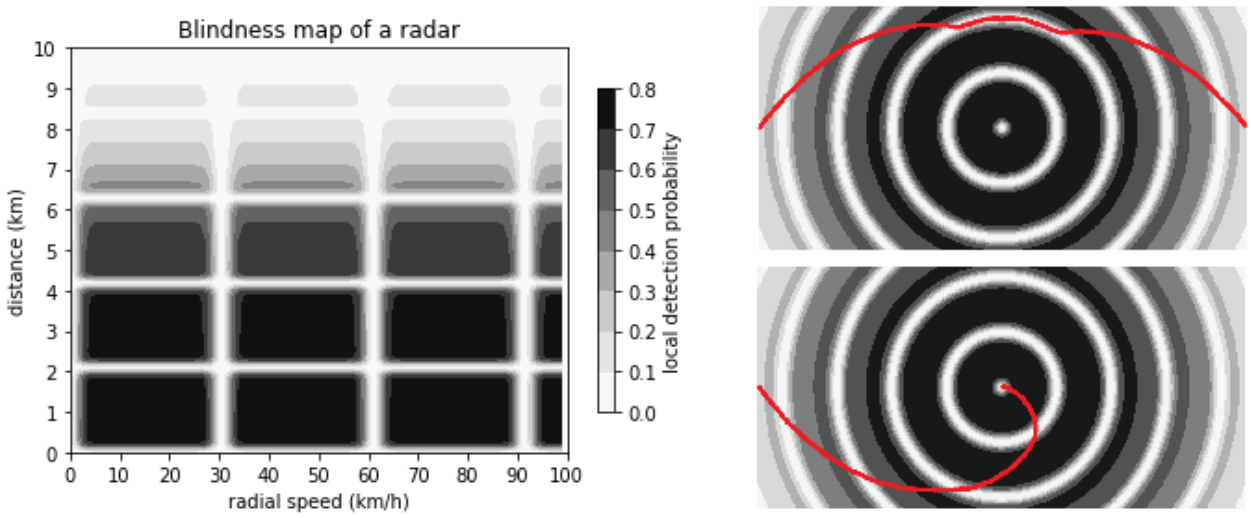

Figure 2.1. (left) blindness map of a radar (simulated data). (top right) dodging a radar through a blind distance, (bottom right) spiraling threatening trajectory.

target, which will take advantage of any hideout in the terrain, blind spot or physical limitation in the radar network. The trajectory is only subject to a lower bound in the turning radius, due to the vehicle high speed (see the companion paper [29]).

We model this problem as a non-cooperative zero-sum game: a first player chooses a setting ξ for the radar detection network Ξ, and the other player chooses a trajectory γ from the admissible class Γ with full information over the network ξ. The players' objective is respectively to maximize and minimize the path cost:

$$C(\Xi, \Gamma) := \sup_{\xi \in \Xi} \inf_{\gamma \in \Gamma} \mathfrak{C}_\xi(\gamma)$$

where $\mathfrak{C}_\xi$ is the function $\mathfrak{C}$ defined in (2.1) but with a data-driven cost term α_ξ depending on the setting ξ of the network, and accounting for the local probability of detection. Minimization over $\gamma \in \Gamma$ (given $\xi \in \Xi$) is performed using the fast and reliable techniques of Section 2.1. We rely on the CMA-ES algorithm [47] for the subsequent optimization over $\xi \in \Xi$, which is rather difficult (non-convex, non-differentiable).

In comparison with earlier works [4, 76], we use the curvature bounded Dubins model (2.2, right) to reject non-physical attacking trajectories, featuring e.g. angular turns or oscillations in the vehicle direction. We also considerably improve, relative to [64], the detection probability model, used to define $\alpha_\xi(\mathbf{x}, \dot{\mathbf{x}})$, taking into account the three following factors respectively related to the radar, the target, and the terrain [73].

- The *blindness map* accounts for the probability of detection of a generic target by a radar, depending on the distance and the radial speed of the target relatively to the radar, see Figure 2.1, left. There are blind areas, due to the fact that a radar cannot listen to its signal while emitting it, and to the Doppler effect, which respectively causes blind radial distances and blind radial speeds. The positions of the blind areas are periodical and depend on internal parameters of the radar that can be optimized: signal wavelength, and pulse repetition interval.

- The *radar cross section* accounts for the probability of detection of a specific target, depending on its orientation relative to the radar. For instance, a furtive plane often has a low probability of detection if seen from the front, and a higher one if seen from the side.

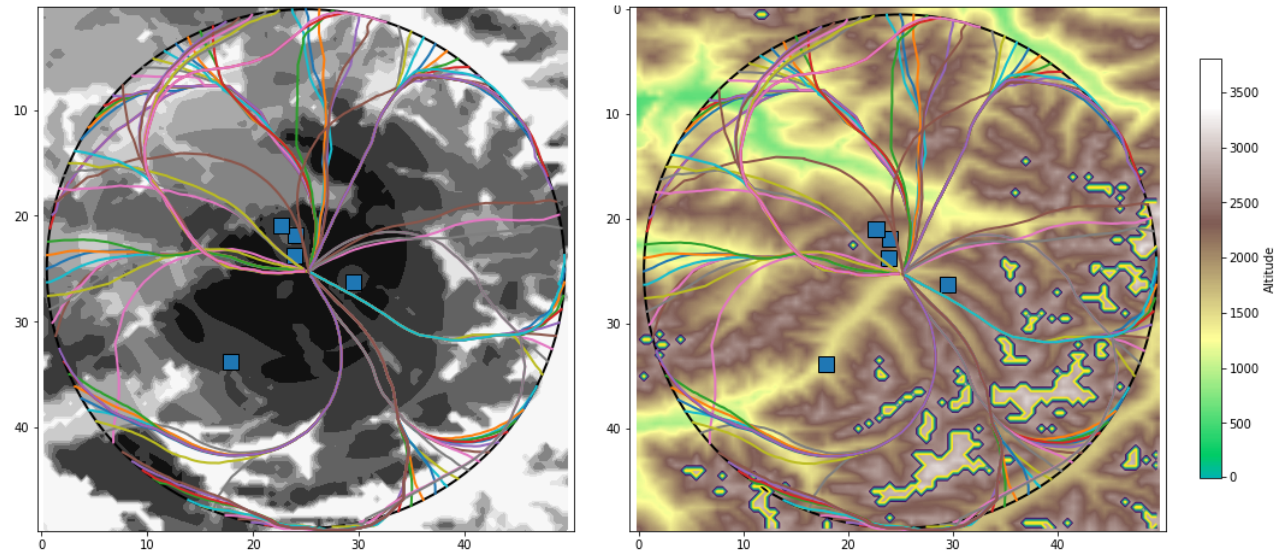

FIGURE 2.2. Threatening trajectories, from a circular region towards its center point, with optimized radar positions. Left: Positional factor $\alpha_\xi(\mathbf{x})$ in the cost map, where ξ is the radar configuration. Right: Digital elevation map.

- The *elevation map* is used to determine blind regions in the terrain due to obstruction of the radar line of sight. In a mountainous area, a target can take advantage of valleys to move "under the radar". The Earth curvature is also taken into account.

The profile of the cost function with regard to the direction of movement is typically non-convex, which is significant only in the presence of a curvature penalization. For that, we choose the Dubins model, in which the curvature radius is bounded. We showcase the following three phenomena.

- Trajectories dodging radars through their blind distances (cf. Figure 2.1, top right). In this picture, only the positional factor in the cost map is shown in greyscale, and not the part of the cost depending on the orientation. The red line represents the optimal trajectory of the target, going from the left to the right of a rectangular domain, with a radar in the center. It features a circle arc, at a precise blind distance from the radar, and two spiral arcs, see below.

- Spiraling threatening trajectories, taking advantage of the blind radial speed (cf. Figure 2.1, bottom right). The red line represents the trajectory of the target, going from the left to the center of the domain where the radar is located, maintaining a constant angle with the radar in order to minimize visibility, except at the end due to the imposed bound on path curvature.

- Hiding in valleys (cf. Figure 2.2). A digital elevation map, of 50km×50km around the city of Davos in the Alps, is used to construct a probability of detection map, see Figure 2.2. Threatening trajectories tend to concentrate in valleys. The optimized radar positions are close to the target to be defended, and either on high ground or in alignment with long valleys.

Future works will be devoted to further enhancing the model, taking into account limited knowledge of the attacker (e.g. due to the use of passive radar receivers), introducing success criteria more complex than mere detection (e.g. requiring detection early enough for interception), and considering speed and altitude variations along the trajectory.

3. Discrete curvatures of point cloud varifolds (by B. Buet, G. P. Leonardi, and S. Masnou)

We sketch in this section the main points allowing to define consistent and stable notions of discrete curvatures on point clouds provided with a varifold structure.

3.1. Introduction

Continuous definitions (of surface, regularity, dimension, curvatures...) generally cannot be transformed directly into their discrete counterpart, especially when dealing with unstructured data such as point clouds. Moreover, these discrete counterparts are generally not unique and highly scale-dependent. Geometric measure theory offers a particularly well-suited framework for the study of such unstructured discrete surfaces. The long-standing Plateau problem has given birth to several different weakenings of the notion of surface. While their common purpose was to gain compactness while preserving mass/area continuity (or lower semi-continuity at least), they actually provide consistent settings for developing a theory of discrete surfaces. We propose to give an insight on a varifold perspective for point cloud processing, as it has been proposed in [17], evidencing good approximation properties in so-called flat distance and a flexible notion of discrete curvature with stability and convergence property with respect to flat distance as well. We insist on the fact that our purpose is not to describe varifolds theory in a general way but quite the reverse, we limit ourselves to the minimal background on varifolds needed for understanding this work, we refer to [72] for general varifolds theory.

3.2. The varifold framework

It is quite natural to associate with a surface a measure that describes it, for instance its area measure, this is also true with a point cloud that can be associated with a sum of Dirac masses. In both cases, there is no loss of information, we can recover the initial object by taking the support of the associated measure. Varifolds push the structure an "order" further, encoding not only the surface M but its whole tangent bundle $TM = \{(x, T_xM), x \in M\}$. We first introduce two sub-classes of varifold structures, namely *point cloud varifolds* and *smooth varifolds*, we will focus on afterwards, then we give an approximation result of smooth varifolds by point cloud ones and eventually we introduce the *flat distance* between varifolds.

Point cloud varifolds and smooth varifolds. Let $d, n \in \mathbb{N}$, $1 \leq d \leq n$ and let us denote by $G_{d,n} = \{d\text{–vector sub-space of } \mathbb{R}^n\}$. Point cloud varifolds and smooth varifolds are d–varifolds, that is:

Definition 3.1 (d–varifold)**.** A d–varifold in $\mathbb{R}^n$ is a Radon measure in $\mathbb{R}^n \times G_{d,n}$.

Thanks to Riesz representation theorem, we can alternatively see varifolds as continuous linear forms on $\mathrm{C}_c(\mathbb{R}^n \times G_{d,n}, \mathbb{R})$ the space of continuous compactly supported functions from $\mathbb{R}^n \times G_{d,n}$ to $\mathbb{R}$. Let us start with *smooth varifolds*

Definition 3.2 (Smooth varifolds)**.** Let $M \subset \mathbb{R}^n$ be a d–sub-manifold, we define $V = v(M)$ by

$$V(B) = \mathcal{H}^d\left(\{x \in M : (x, T_xM) \in B\}\right), \quad \text{for all Borel sets } B \subset \mathbb{R}^n \times G_{d,n}\,,$$

where $\mathcal{H}^d$ denotes the d–dimensional Hausdorff measure, or equivalently as the continuous linear form

$$V(\phi) = \int_M \phi(x, T_xM)\, \mathrm{d}\mathcal{H}^d(x) \quad \text{for all } \phi \in \mathrm{C}_c(\mathbb{R}^n \times G_{d,n}, \mathbb{R})\,.$$

Loosely speaking, $v(M)$ is the natural measure exactly supported in TM. Let us give some examples.

- Let $\Gamma \subset \mathbb{R}^2$ be a closed regular curve parametrized by $\gamma : [0, L] \to \mathbb{R}^2$ with unit speed : $\|\gamma'(t)\| = 1$. Following Definition 3.2, the smooth varifold $V = v(D)$ associated with Γ acts on continuous functions $\phi \in \mathrm{C}_c(\mathbb{R}^2 \times \mathrm{G}_{1,2})$ through
$$V(\phi) = \int_\Gamma \phi(x, T_x\Gamma)\, \mathrm{d}\mathcal{H}^1(x) = \int_{t=0}^{L} \phi(\gamma(t), \operatorname{span} \gamma'(t))\, \mathrm{d}t \tag{3.1}$$
- If we consider a line $D \subset \mathbb{R}^n$, the tangent line is the same for all $x \in D$: $T_xD = D$. In this case the varifold $V = v(D)$ can be decomposed into a tensor product of a first measure $\mathcal{H}^1_{\lfloor D}$ (i.e. the length measure on the line D) in $\mathbb{R}^n$ and a second measure δ_D in $\mathrm{G}_{1,n}$, such a measure is usually denoted by $V = \mathcal{H}^1_{\lfloor D} \otimes \delta_D$. Such a decomposition is in general impossible. When it exists, this means that one can separate integration with respect to $\mathbb{R}^n$ and $G_{d,n}$ and indifferently switch integration order. Yet, on the curve Γ, the tangential direction generally depends on the position in the curve.

Notice that smooth varifolds are obviously a particular case of so called *rectifiable varifolds* for which one only requires the existence of an approximate tangent plane almost everywhere. Typical examples of such varifolds are associated with Lipschitz graphs, allowing for instance corners or edges.

Definition 3.3 (Point cloud varifolds)**.** Let $X = \{x_i\}_{i=1\dots N} \subset \mathbb{R}^n$ be a finite set of points in $\mathbb{R}^n$, $(m_i)_{i=1\dots N} \subset \mathbb{R}_+$ be associated weights and $(P_i)_{i=1\dots N} \subset G_{d,n}$ be associated directions. Then, define $V = v(X)$ as the weighted sum of Dirac masses $V = \sum_{i=1}^N m_i \delta_{(x_i, P_i)}$.

In particular for $V = v(X)$, $V(B) = \sum_{i=1}^N m_i \chi_B(x_i, P_i)$ for B Borel set, and $V(\phi) = \sum_{i=1}^N m_i \phi(x_i, P_i)$ for $\phi \in \mathrm{C}(\mathbb{R}^n \times G_{d,n}, \mathbb{R})$. Note that while $v(M)$ is uniquely defined from M when M is a d–sub-manifold since TM is uniquely defined from M, this is false for point cloud varifolds, $v(X)$ is not uniquely defined from the positions $X = \{x_i\}_{i=1\dots N}$ since there is not a unique way of defining $m_i, P_i, i = 1 \dots N$ from X.

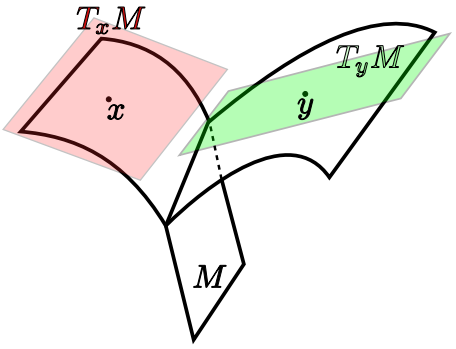

(a) A rectifiable varifold.

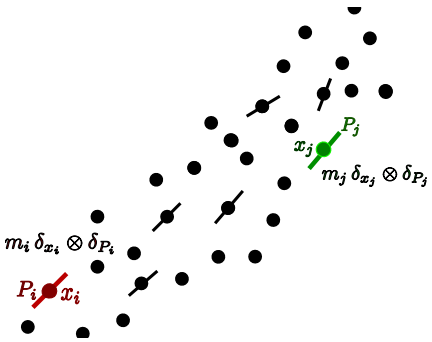

(b) A point cloud varifold.

Notice that we recover the spatial measure (i.e. $\mathcal{H}^d_{\lfloor M}$ for a smooth varifold and $\sum_i m_i \delta_{x_i}$ for a point cloud varifold) by defining the *mass* $\|V\|$ of V as follows:

Definition 3.4 (Mass)**.** Given a d–varifold in $\mathbb{R}^n$, we define its *mass* $\|V\|$ as the Radon measure in $\mathbb{R}^n$ such that for all $B \subset \mathbb{R}^n$ Borel set, $\|V\|(B) = V(B \times G_{d,n})$.

Approximation in weak star topology. As both point clouds and sub-manifolds are now endowed with a structure of d–varifolds, we can use topologies/distances between varifolds to compare them, hoping that in some topology, we have built a good framework of approximation, meaning that it

is possible to approximate a d–submanifold M by point clouds in this topology. Again by Riesz theorem, varifolds are the dual of $\mathrm{C}_c(\mathbb{R}^n \times G_{d,n}, \mathbb{R})$ and thus inherit of a weak star topology induced by $\mathrm{C}_c(\mathbb{R}^n \times G_{d,n}, \mathbb{R})$. To be more explicit, a sequence of d–varifolds $(V_h)_h$ weak star converge to V if and only if $V_h(\phi) \xrightarrow[h\to\infty]{} V(\phi)$ for all $\phi \in \mathrm{C}_c(\mathbb{R}^n \times G_{d,n}, \mathbb{R})$. Let us give a first result ensuring that weak star topology provides a consistent framework of approximation:

Theorem 3.5. *Let $V = v(M)$ be a smooth d–varifold in $\mathbb{R}^n$, then there exists a sequence of point cloud d–varifolds $(V_h)_h$ that weak star converges to V.*

This approximation result still holds when replacing the smooth d–varifold by any d–rectifiable varifold.

Flat distance. Let us now introduce a distance that locally metrizes weak star topology in the sense of Theorem 3.7.

Definition 3.6 (Flat distance)**.** Let V, W be d–varifolds in $\mathbb{R}^n$ and $B \subset \mathbb{R}^n$ be an open set. We introduce

$$\Delta_B(V,W) := \sup \left\{ \int_{\mathbb{R}^n \times G_{d,n}} \phi \,\mathrm{d}V - \int_{\mathbb{R}^n \times G_{d,n}} \phi \,\mathrm{d}W \;\middle|\; \begin{array}{l} \phi \in \mathrm{C}_c(\mathbb{R}^n \times G_{d,n}, \mathbb{R}) \text{ is 1–Lipschitz} \\ \sup_{\mathbb{R}^n \times G_{d,n}} |\phi| \leq 1 \\ \operatorname{spt} \phi \subset B \times G_{d,n} \end{array} \right\}.$$

When $B = \mathbb{R}^n$, $\Delta_{\mathbb{R}^n}$ (simply denoted by Δ) is the *flat distance* or also known as *bounded Lipschitz distance*.

Let us consider two simple examples of 1–varifolds in $\mathbb{R}$ in order to understand the restriction on test functions in Definition 3.6, starting with the assumption ϕ 1–Lipschitz. Consider $V_0 = \delta_{(0,\mathbb{R})}$ and for $\epsilon > 0$, $V_\epsilon = \delta_{(\epsilon,\mathbb{R})}$ two 1–varifolds in $\mathbb{R}$, then $\Delta(V_0, V_\epsilon) \geq |\psi(0) - \psi(\epsilon)|$ (with any $\psi \in \mathrm{C}_c(\mathbb{R}, \mathbb{R})$ and $\phi(x, S) = \psi(x) \in \mathrm{C}_c(\mathbb{R} \times G_{1,1}, \mathbb{R})$). If there is no control on the slope of the test function, then taking $\psi(0) = 1$ and $\psi(\epsilon) = -1$, we get $\Delta(V_0, V_\epsilon) \geq 2$ independently of $\epsilon > 0$, which is really bad for approximation purposes. If we now remove the assumption $|\phi| \leq 1$, then for $\epsilon > 0$, $\Delta(V_0, (1+\epsilon)V_0) \geq \epsilon|\phi(0, \mathbb{R})|$ and thus is infinite if ϕ is not bounded, which is also bad. While we evidenced with toy examples the soundness of those two restrictions on test functions $\phi \in \mathrm{C}_c(\mathbb{R}^n \times G_{d,n}, \mathbb{R})$, they turn out to be sufficient, in the sense that Δ metrizes weak star convergence in compact sets, as stated in next theorem.

Theorem 3.7 ([9])**.** *Let $(V_h)_h$, V be d–varifolds in $\mathbb{R}^n$ such that $\sup_h V_h(\mathbb{R}^n) + V(\mathbb{R}^n) < \infty$ and assume that there exists a compact set $K \subset \mathbb{R}^n$ such that $\operatorname{spt} V$, $\operatorname{spt} V_h \subset K \times G_{d,n}$ for all $h \in \mathbb{N}$. Then,*

$$V_h \text{ weak star converges to } V \quad \Leftrightarrow \quad \Delta(V, V_h) \xrightarrow[h\to\infty]{} 0\,.$$

3.3. **Discrete mean curvature**

Our purpose is now to introduce discrete curvatures, starting with discrete mean curvature, whose convergence holds with respect to weak star convergence of point cloud varifolds (to a smooth varifold). We first introduce the notions that generalize mean curvature for d–varifolds, we then adapt it to point cloud and eventually state convergence results.

First variation and generalized mean curvature. Let us start with a smooth d–varifold $V = v(M)$ associated with a smooth closed d–sub-manifold M. By its very definition, V encodes TM, that is order 1 information about M. It is then reasonable to expect mean curvature to rewrite as a

distributional derivative of order 1 of V. Indeed, consider the order 1 distribution $\delta V : \mathrm{C}^1_c(\mathbb{R}^n, \mathbb{R}^n) \to \mathbb{R}$ defined as

$$\delta V(X) = \int_M \mathrm{div}_{T_x M} X(x)\, \mathrm{d}\mathcal{H}^d(x) \underbrace{=}_{\substack{\text{divergence}\\ \text{theorem}}} -\int_M \underbrace{H(x)}_{\substack{\text{mean curvature}\\ \text{vector of } M}} \cdot X(x)\, \mathrm{d}\mathcal{H}^d(x)\,. \tag{3.2}$$

What is important in (3.2) is that the distribution δV encodes mean curvature and entirely relies on varifold structure $v(M)$ we defined on M. For this last reason, it can be extended to any d–varifold as follows:

Definition 3.8 (First variation, [1])**.** Let V be a d–varifold in $\mathbb{R}^n$, we define for $X \in \mathrm{C}^1_c(\mathbb{R}^n, \mathbb{R}^n)$,

$$\delta V(X) = \int_{(x,S)\in\mathbb{R}^n\times G_{d,n}} \mathrm{div}_S X(x)\, \mathrm{d}V(x,S) \quad \text{with} \quad \begin{cases} \mathrm{div}_S X(x) = \sum_{i=1}^n DX(x)\tau_i \cdot \tau_i, \\ (\tau_1, \dots, \tau_d) \text{ orthon. basis of } S \in G_{d,n}. \end{cases}$$

δV is a distribution of order 1 called *first variation* of V.

As we saw in (3.2), if $V = v(M)$ with M smooth and closed, then δV identifies with the (vector) Radon measure $-H\mathcal{H}^d_{|M} = -H\|V\|$, and H is the Radon–Nikodym derivative of $-\delta V = H\mathcal{H}^d_{|M}$ with respect to $\|V\| = \mathcal{H}^d_{|M}$. As soon as δV identifies with a Radon measure (which can be reformulated as δV being continuous with respect to $\mathrm{C}_c(\mathbb{R}^n, \mathbb{R}^n)$ topology), it is similarly possible to define a generalized mean curvature vector.

Definition 3.9 (Generalized mean curvature)**.** Let V be a d–varifold in $\mathbb{R}^n$ and assume that δV is a Radon measure. Then define $H(\,\cdot\,, V) \in \mathrm{L}^1(\mathbb{R}^n, \|V\|)$ as the Radon–Nikodym derivative of $-\delta V$ with respect to $\|V\|$. It is called *generalized mean curvature vector*.

Let us come back to the example of smooth varifold $V = v(\Gamma)$ introduced in (3.1). Let $X \in \mathrm{C}^1_c(\mathbb{R}^2, \mathbb{R}^2)$, then recalling the action of V on continuous functions and applying it with $(x, S) \mapsto \mathrm{div}_S\, X(x)$, we obtain

$$\begin{aligned} \delta V(X) &= \int \mathrm{div}_S\, X(x)\, \mathrm{d}V(x,S) = \int_{t=0}^L \mathrm{div}_{\mathrm{span}\,\gamma'(t)}\, X(\gamma(t))\, \mathrm{d}t = \int_{t=0}^L DX(\gamma(t))\gamma'(t)\cdot\gamma'(t)\, \mathrm{d}t \\ &= \int_0^L \frac{\mathrm{d}}{\mathrm{d}t} X(\gamma(t))\cdot\gamma'(t)\, \mathrm{d}t = -\int_{t=0}^L X(\gamma(t))\cdot \underbrace{\gamma''(t)}_{\kappa(\gamma(t))}\, \mathrm{d}t \qquad (3.3) \\ &= -\int_\Gamma X\cdot\kappa\,. \qquad (3.4) \end{aligned}$$

Notice that in this case, divergence theorem reduces to the classical by parts integration (3.3). By definition, the generalized mean curvature directly reads on (3.4) as κ and recalling that γ is an arc-length parametrization γ'' is indeed the curvature.

Unfortunately, if V is a point cloud d–varifold, there is no hope that δV is a Radon measure. Indeed, in $\mathbb{R}$, let $V = \delta_{(0,\mathbb{R})}$ and $X \in \mathrm{C}^1_c(\mathbb{R}, \mathbb{R})$, one can check that $\delta V(X) = X'(0) = -(\delta_0)'(X)$ and it is well-known (and easy to check) that $(\delta_0)'$ is not a Radon measure. We introduce a regularization via convolution of δV in order to overcome this lack of regularity of the first variation of point clouds.

Discrete mean curvature. Let $\rho : \mathbb{R} \to \mathbb{R}_+ \in \mathrm{C}^\infty(\mathbb{R})$ be even and compactly supported in $(-1, 1)$ and define $(\rho_\epsilon)_{\epsilon>0}$ in $\mathbb{R}^n$ by $\rho_\epsilon(x) = \epsilon^{-n}\rho(|x|/\epsilon)$. The regularized linear form $\delta V * \rho_\epsilon$ then identifies to a smooth and locally integrable function in $\mathbb{R}^n$ whose expression is

$$\delta V * \rho_\epsilon(x) = \frac{1}{\epsilon^{n+1}} \int_{\mathbb{R}^n\times G_{d,n}} \rho'\left(\frac{|y-x|}{\epsilon}\right) \Pi_S\left(\frac{y-x}{|y-x|}\right) \mathrm{d}V(y,S)\,, \quad x \in \mathbb{R}^n \tag{3.5}$$

where Π_S is the orthogonal projection onto the d–plane $S \in G_{d,n}$.

So as to define a mean curvature from this regularized first variation, we follow the definition of $H(\,\cdot\,, V)$ as a Radon–Nikodym, and we consequently define $H_\epsilon(\,\cdot\,, V)$ as the Radon–Nikodym derivative of $\delta V * \rho_\epsilon$ with respect to $\|V\| * \xi_\epsilon$ (where ξ_ϵ is define similarly to ρ_ϵ from a smooth positive and even profile ξ compactly supported in $(-1, 1)$). Now, the Radon–Nikodym derivative of two measures that are absolutely continuous with respect to Lebesgue measure is simply the quotient of the associated densities:

Definition 3.10 (ϵ–mean curvature [17, 4.1])**.** Let V be a d–varifold in $\mathbb{R}^n$, for $x \in \mathbb{R}^n$ and $\epsilon > 0$, we define

$$H_\epsilon(x, V) = -\frac{1}{C_{\rho,\xi}} \frac{\delta V * \rho_\epsilon(x)}{\|V\| * \xi_\epsilon(x)}\,, \tag{3.6}$$

the constant $C_{\rho,\xi} > 0$ explicitly depends on ρ and ξ.

First of all, Definition 3.10 is consistent for smooth varifolds $V = v(M)$ (and more generally rectifiable varifolds whose first variation is a Radon measure) in the sense that for $x \in M$,

$$H_\epsilon(x, V) \xrightarrow[\epsilon \to 0]{} H(x) = H(x, V)\,.$$

Furthermore, choosing ρ and ξ satisfying $s\rho'(s) + n\xi(s) = 0$ allow to stabilize numerical computations since it cancels the integrand of the first order term in the expansion of $|H_\epsilon - H|$, which is generally zero only due to by parts integration. In this case $C_{\rho,\xi} = n/d$.

More than consistency, we have the following stability (and convergence follows directly from both consistency and stability) theorem:

Theorem 3.11 ([17, Thm. 4.5])**.** *Let $V = v(M)$ be a smooth d–varifold associated with a closed smooth d–sub-manifold M, H its mean curvature vector. Let $x \in M$ and assume that*

- *$(z_h)_h$ is a sequence of points in $\mathbb{R}^n$ tending to x.*
- *$(V_h)_h$ is a sequence of d–varifolds in $\mathbb{R}^n$ such that $\exists\, \eta_h \downarrow 0$,*

$$d_h = \sup\left\{ \frac{\Delta_B(V, V_h)}{\min\left(\|V\|(B^{\eta_h}), \|V_h\|(B^{\eta_h})\right)} \;\middle|\; \begin{array}{l} B = B(x, r) \text{ ball centered at } x \in M \\ B(x, r)^{\eta_h} = B(x, r + \eta_h) \end{array} \right\} \xrightarrow[h \to +\infty]{} 0\,.$$

Then, for $\epsilon_h \downarrow 0$ satisfying $\frac{d_h + |z_h - x| + \eta_h}{\epsilon_h^2} \xrightarrow[h \to \infty]{} 0$,

$$|H_{\epsilon_h}(z_h, V_h) - H_{\epsilon_h}(x, V)| = O_{h \to \infty}\left(\frac{d_h + |z_h - x|}{\epsilon_h^2}\right)$$

Eventually, let us insist on the fact that Definition 3.10 rewrites "simply" for a point cloud varifold as it only involves computations of ϵ–neighbourhoods and elementary operations. More precisely, for

$$V = \sum_{i=1}^N m_i \delta_{(x_i, P_i)}, \quad \text{we obtain} \quad H_\epsilon(x, V) = -\frac{\dfrac{d}{n\epsilon} \displaystyle\sum_{i=1}^N m_i \rho'\left(\frac{|x_i - x|}{\epsilon}\right) \frac{\Pi_{P_i}(x_i - x)}{|x_i - x|}}{\displaystyle\sum_{i=1}^N m_i \xi\left(\frac{|x_i - x|}{\epsilon}\right)}.$$

3.4. **Discrete second fundamental form**

We now address the question of recovering from the varifold structure not only the mean curvature vector but the whole second fundamental form (whose mean curvature is the trace). In this section, we give an overview of the path leading to a notion of weak second fundamental form as a family of linear distribution of order 1 allowing to recover similar convergence properties as for mean curvature (see [18]). To this end, we consider Hutchinson's weak notion of second fundamental form (see [49]) that consists in testing divergence theorem on vector fields X now depending both on $x \in \mathbb{R}^n$ and $S \in G_{d,n}$. However, our motivation differs from Hutchinson's, who gave a weak notion of second fundamental form, but strong enough to ensure that its L^p–control implies strong regularity ([48]): the varifold is then at every point of its support (locally) a finite union of graphs thus excluding triple junctions in $\mathbb{R}^2$ for instance. In contrast we aim at defining a discrete second fundamental form with good properties of convergence, similar to Theorem 3.11. That is the reason why we consider only test functions depending linearly on $S \in G_{d,n}$, that is functions of the form $S_{jk}X(x) = S_{jk}\phi(x)e_i$ for $i,j,k = 1\dots n$ and $(e_1,\dots,e_n)$ the canonical basis of $\mathbb{R}^n$. On one hand we lose Hutchinson's regularity results, but on the other hand we obtain a notion of second fundamental form to which similar techniques as for the mean curvature may be applied.

Let us start with smooth varifolds. Let M be a closed and smooth d–sub-manifold and let $V = v(M)$, then for all $i,j,k = 1\dots n$ and every $\phi \in \mathrm{C}^1_c(\mathbb{R}^n,\mathbb{R})$, the following by parts integration formula hold:

$$-\int_M (\Pi_{T_xM}\nabla\phi)_i \,\mathrm{d}\mathcal{H}^d = \int_M \Big(A_{ijk}\phi + (T_xM)_{jk}\sum_q A_{qiq}\phi\Big)\,\mathrm{d}\mathcal{H}^d$$
$$\text{with}\quad A_{ijk}(x) = e_i\cdot\Pi_{T_xM}\nabla\{x\mapsto(T_xM)_{jk}\}$$

We can thus define the weak second fundamental form of V as soon as for $i,j,k = 1\dots n$, the following linear forms $\delta_{ijk}V$ are Radon measures

$$\delta_{ijk}V : \phi \in \mathrm{C}^1_c(\mathbb{R}^n,\mathbb{R}) \longmapsto e_i\cdot\int_{\mathbb{R}^n\times G_{d,n}} S_{jk}\Pi_S\nabla\phi(x)\,\mathrm{d}V(x,S)\,.$$

In this case, we can take the Radon–Nikodym derivative $\beta_{ijk} \in \mathrm{L}^1_{loc}(\|V\|)$ of $-\delta_{ijk}V$ with respect to $\|V\|$, $\beta_{ijk} = -\frac{\delta_{ijk}V}{\|V\|}$. For $x \in M$, $A_{ijk}(x)$ is then defined as the unique solution of the system with n^3 equations:

$$A_{ijk} + c_{jk}\sum_{q=1}^n A_{qiq} = \beta_{ijk} \quad\text{with}\quad c_{jk}(x) = T_xM\,.$$

It is then possible to recover the extended second fundamental form $B^k_{ij} = B(e_i^T,e_j^T)\cdot e_k$ by $B^k_{ij} = \frac{1}{2}\left(A_{ijk} + A_{jik} - A_{kij}\right)$. At this stage, it "only" remains to regularize $\delta_{ijk}V$ via convolution and define for $\epsilon > 0$, $(\beta_{ijk})^\epsilon$, $(c_{jk})^\epsilon$ as

$$\beta^\epsilon_{ijk} = -\frac{\delta_{ijk}V * \rho_\epsilon}{\|V\| * \xi_\epsilon} \quad\text{and}\quad c^\epsilon_{jk}(x) = \frac{\int_{\mathbb{R}^n\times G_{d,n}} S_{jk}\zeta_\epsilon(y-x)\,\mathrm{d}V(y,S)}{\|V\| * \zeta_\epsilon(x)}$$

and eventually A^ϵ_{ijk} as solution of the regularized system. In doing so, we obtain the same consistency and stability properties as for the ϵ–mean curvature.

Figure 3.1 shows two examples of curvature approximation on 3D point clouds. In future work, we plan to apply these techniques to more general data in arbitrary dimension and codimension for classification, analysis or denoising purposes. Another possible extension is the approximation of second-order derivatives of irregularly sampled functions, which might be useful for various grid-free numerical methods.

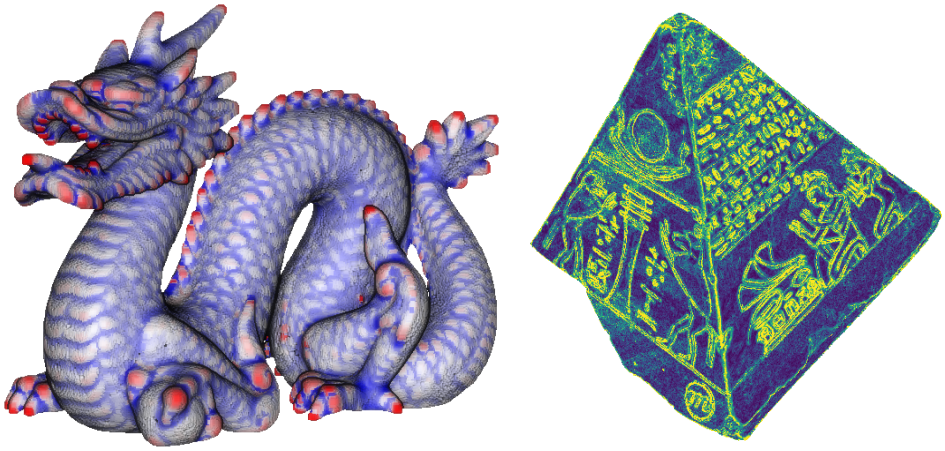

FIGURE 3.1. Left: Gaussian curvature $\kappa_1\kappa_2$ computed on a $3D$ point clouds from Stanford repository `http://graphics.stanford.edu/data/3Dscanrep/`, from negative values (blue) to positive ones (red) passing through null values (white), Right: Sum of absolute values of principal curvatures $|\kappa_1| + |\kappa_2|$ computed on a $3D$ point cloud from Farman Institute 3D Point Sets [28], from null values (blue) to high positive ones (yellow) passing through green.

References

[1] W. K. Allard. On the first variation of a varifold. *Ann. Math.*, 95:417–491, 1972.

[2] F. Almgren, J. E. Taylor, and L. Wang. Curvature-driven flows: a variational approach. *SIAM J. Control Optimization*, 31(2):387–438, 1993.

[3] C. R. Anderson. A Rayleigh–Chebyshev procedure for finding the smallest eigenvalues and associated eigenvectors of large sparse Hermitian matrices. *J. Comput. Phys.*, 229(19):7477–7487, 2010.

[4] F. Barbaresco. Computation of most threatening radar trajectories areas and corridors based on fast-marching & level sets. In *IEEE Symposium on Computational Intelligence for Security and Defence Applications*, pages 51–58, 2011.

[5] M. Bardi and I. Capuzzo-Dolcetta. *Optimal control and viscosity solutions of Hamilton–Jacobi–Bellman equations*. Modern Birkhäuser Classics. Birkhäuser, 2008.

[6] G. Barles and C. Georgelin. A simple proof of convergence for an approximation scheme for computing motions by mean curvature. *SIAM J. Numer. Anal.*, 32(2):484–500, 1995.

[7] G. Barles, H. M. Soner, and P. E. Souganidis. Front propagation and phase field theory. *SIAM J. Control Optimization*, 31(2):439–469, 1993.

[8] A. L. Bertozzi and A. Flenner. Diffuse interface models on graphs for analysis of high dimensional data. *SIAM J. Multiscale Mod. Simul.*, 10(3):1090–1118, 2012.

[9] V. I. Bogachev. *Measure Theory II*. Springer, 2007.

[10] J. Boschand, S. Klamt, and M. Stoll. Generalizing diffuse interface methods on graphs: non-smooth potentials and hypergraphs. *SIAM J. Appl. Math.*, 78(3):1350–1377, 2018.

[11] A. Braides. Γ-*convergence for beginners*. Oxford University Press, 2002.

[12] K. A. Brakke. *The motion of a surface by its mean curvature*. Princeton University Press, 1978.

[13] X. Bresson and T. F. Chan. Non-local Unsupervised Variational Image Segmentation. Technical report, UCLA, 2008. cam-08-67.

[14] L. Bronsard and R. V. Kohn. Motion by mean curvature as the singular limit of Ginzburg–Landau dynamics. *J. Differ. Equations*, 90(2):211–237, 1991.

[15] J. Budd and Y. van Gennip. Mass-preserving diffusion-based dynamics on graphs. in preparation.

[16] J. Budd and Y. van Gennip. Graph MBO as a semi-discrete implicit Euler scheme for graph Allen–Cahn. `https://arxiv.org/abs/1907.10774`, 2019.

[17] B. Buet, G. P. Leonardi, and S. Masnou. A varifold approach to surface approximation. *Arch. Ration. Mech. Anal.*, 226:639–694, 2017.

[18] B. Buet, G. P. Leonardi, and S. Masnou. Weak and approximate curvatures of a measure: a varifold perspective. submitted, 2019.

[19] L. Calatroni, Y. van Gennip, C.-B. Schönlieb, H. Rowland, and A. Flenner. Graph clustering, variational image segmentation methods and Hough transform scale detection for object measurement in images. *J. Math. Imaging Vis.*, 57(2):269–291, 2017.

[20] J. Calder. Consistency of Lipschitz learning with infinite unlabeled data and finite labeled data. `https://arxiv.org/abs/1710.10364`, 2017.

[21] J. Calder. The game theoretic p-Laplacian and semi-supervised learning with few labels. *Nonlinearity*, 32(1):301–330, 2018.

[22] J. Calder and D. Slepčev. Properly-weighted graph Laplacian for semi-supervised learning. `https://arxiv.org/abs/1810.04351`, 2018.

[23] D. Chen, J.-M. Mirebeau, and L. D. Cohen. Global minimum for a Finsler Elastica minimal path approach. *Int. J. Comput. Vision*, 122(3):458–483, 2017.

[24] F. Chung. *Spectral Graph Theory*. American Mathematical Society, 1997.

[25] L. D. Cohen and R. Kimmel. Global minimum for active contour models: A minimal path approach. *Int. J. Comput. Vision*, 24(1):57–78, 1997.

[26] M. Cucuringu, A. Pizzoferrato, and Y. van Gennip. An MBO scheme for clustering and semi-supervised clustering of signed networks. `https://arxiv.org/abs/1901.03091`, 2019.

[27] G. Dal Maso. *An introduction to* Γ*-convergence*. Birkhäuser, 1993.

[28] J. Digne, N. Audfray, C. Lartigue, C. Mehdi-Souzani, and J.-M. Morel. Farman Institute 3D Point Sets - High Precision 3D Data Sets. *IPOL Journal*, 1:281–291, 2011.

[29] J. Dreo, F. Desquilbet, F. Barbaresco, and J.-M. Mirebeau. Netted multi-function radars positioning and modes selection by non-holonomic fast marching computation of highest threatening trajectories. In *International RADAR'19 conference*. IEEE, 2019.

[30] R. Duits, S. P. L. Meesters, J.-M. Mirebeau, and J. M. Portegies. Optimal paths for variants of the 2D and 3D Reeds–Shepp car with applications in image analysis. *J. Math. Imaging Vis.*, pages 1–33, 2018.

[31] M. M. Dunlop, D. Slepčev, A. M. Stuart, and M. Thorpe. Large data and zero noise limits of graph-based semi-supervised learning algorithms. `https://arxiv.org/abs/1805:09450`, 2018.

[32] A. Elmoataz and P. Buyssens. On the connection between tug-of-war games and nonlocal PDEs on graphs. *C. R. Méc. Acad. Sci. Paris*, 345(3):177–183, 2017.

[33] A. Elmoataz, X. Desquesnes, and O. Lézoray. Non-local morphological PDEs and p-Laplacian equation on graphs with applications in image processing and machine learning. *IEEE Sel. Top. Signal Process.*, 6(7):764–779, 2012.

[34] A. Elmoataz, X. Desquesnes, and M. Toutain. On the game p-Laplacian on weighted graphs with applications in image processing and data clustering. *Eur. J. Appl. Math.*, 28:922–948, 2017.

[35] L. C. Evans. Convergence of an algorithm for mean curvature motion. *Indiana Univ. Math. J.*, 42(2):533–557, 1993.

[36] C. Fowlkes, S. Belongie, F. Chung, and J. Malik. Spectral grouping using the Nystrom method. *IEEE Trans. Pattern Anal. Mach. Intell.*, 26(2):214–225, 2004.

[37] C. Garcia-Cardona, A. Flenner, and A. G. Percus. Multiclass diffuse interface models for semi-supervised learning on graphs. In *Proceedings of the 2nd International Conference on Pattern Recognition Applications and Methods (ICPRAM 2013)*, pages 78–86, 2013.

[38] C. Garcia-Cardona, A. Flenner, and A. G. Percus. Multiclass semi-supervised learning on graphs using Ginzburg–Landau functional minimization. *Adv. Intell. Syst. Comput.*, 318:19–135, 2015.

[39] C. Garcia-Cardona, E. Merkurjev, A. L. Bertozzi, A. Flenner, and A. G. Percus. Multiclass data segmentation using diffuse interface methods on graphs. *IEEE Trans. Pattern Anal. Mach. Intell.*, 36:1600–1613, 2014.

[40] N. Garcia Trillos and R. Murray. A new analytical approach to consistency and overfitting in regularized empirical risk minimization. *Eur. J. Appl. Math.*, 28:886–921, 2017.

[41] N. Garcia Trillos and R. Murray. A maximum principle argument for the uniform convergence of graph Laplacian regressors. `https://arxiv.org/abs/1901.10089`, 2019.

[42] N. Garcia Trillos and D. Slepčev. Continuum limit of total variation on point clouds. *Arch. Ration. Mech. Anal.*, 220(1):193–241, 2016.

[43] N. Garcia Trillos, D. Slepčev, J. von Brecht, T. Laurent, and X. Bresson. Consistency of Cheeger and Ratio Graph Cuts. *J. Mach. Learn. Res.*, 17:1–46, 2016.

[44] G. Gilboa and S. J. Osher. Nonlocal Operators with Applications to Image Processing. *SIAM J. Multiscale Mod. Simul.*, 7(3):1005–1028, 2008.

[45] Y. Hafiene, J. Fadili, and A. Elmoataz. Nonlocal p-Laplacian evolution problems on graphs. *SIAM J. Numer. Anal.*, 56(2):1064–1090, 2018.

[46] Y. Hafiene, J. Fadili, and A. Elmoataz. Nonlocal p-Laplacian variational problems on graphs. `https://arxiv.org/abs/1810.12817`, 2018.

[47] N. Hansen, S. D. Müller, and P. Koumoutsakos. Reducing the time complexity of the derandomized evolution strategy with covariance matrix adaptation (CMA-ES). *Evol. Comput.*, 11(1):1–18, 2003.

[48] J. E. Hutchinson. $C^{1,\alpha}$ multiple function regularity and tangent cone behaviour for varifolds with second fundamental form in L^p. In *Geometric measure theory and the calculus of variations*, volume 44 of *Proceedings of Symposia in Pure Mathematics*. American Mathematical Society, 1986.

[49] J. E. Hutchinson. Second fundamental form for varifolds and the existence of surfaces minimising curvature. *Indiana Univ. Math. J.*, 35(1), 1986.

[50] M. Kass, A. Witkin, and D. Terzopoulos. Snakes: Active contour models. *Int. J. Comput. Vision*, 14:321–331, 1988.

[51] B. Keetch and Y. van Gennip. Approximation of the Max-K-Cut via a signless graph Allen–Cahn equation. In preparation.

[52] B. Keetch and Y. van Gennip. A Max-Cut approximation using a graph based MBO scheme. `https://arxiv.org/abs/1711.02419`, 2017.

[53] W. Liao, K. Rohr, and S. Wörz. Globally Optimal Curvature - Regularized Fast Marching For Vessel Segmentation,. In *Medical Image Computing and Computer-Assisted Intervention - MICCAI 2013*, pages 550–557. Springer, 2013.

[54] F. Lozes, M. Hidane, A. Elmoataz, and O. Lezoray. Nonlocal segmentation of point clouds with graphs. In *2013 IEEE Global Conference on Signal and Information Processing, GlobalSIP 2013 - Proceedings*, pages 459–462, 2013.

[55] S. Luckhaus and T. Sturzenhecker. Implicit time discretization for the mean curvature flow equation. *Calc. Var. Partial Differ. Equ.*, 3(2):253–271, 1995.

[56] X. Luo and A. L. Bertozzi. Convergence of the graph Allen–Cahn scheme. *J. Stat. Phys.*, 167(3):934–958, 2017.

[57] J. J. Manfredi, A. M. Oberman, and A. P. Sviridov. Nonlinear elliptic partial differential equations and p-harmonic functions on graphs. *Differ. Integral Equ.*, 28(1–2):79–102, 2015.

[58] G. S. Medvedev. The nonlinear heat equation on dense graphs and graph limits. *SIAM J. Math. Anal.*, 46(4):2743–2766, 2014.

[59] Z. Meng, E. Merkurjev, A. Koniges, and A. L. Bertozzi. Hyperspectral Image Classification Using Graph Clustering Methods. *IPOL Journal*, 7:218–245, 2017.

[60] E. Merkurjev, C. Garcia-Cardona, A. L. Bertozzi, A. Flenner, and A. G. Percus. Diffuse interface methods for multiclass segmentation of high-dimensional data. *Appl. Math. Lett.*, 33:29–34, 2014.

[61] E. Merkurjev, T. Kostic, and A. L. Bertozzi. An MBO scheme on graphs for segmentation and image processing. *SIAM J. Imaging Sci.*, 6(4):1903–1930, 2013.

[62] B. Merriman, J. K. Bence, and S. J. Osher. Motion of multiple functions: a level set approach. *J. Comput. Phys.*, 112(2):334–363, 1994.

[63] J.-M. Mirebeau. Fast-marching methods for curvature penalized shortest paths. *J. Math. Imaging Vis.*, pages 1–32, 2017.

[64] J.-M. Mirebeau and J. Dreo. Automatic differentiation of non-holonomic fast marching for computing most threatening trajectories under sensors surveillance. In *Geometrical Science of Information*, 2017.

[65] J.-M. Mirebeau and J. M. Portegies. Hamiltonian fast marching: A numerical solver for anisotropic and non-holonomic eikonal PDEs. *IPOL Journal*, 9:47–93, 2019.

[66] L. Modica. The gradient theory of phase transitions and the minimal interface criterion. *Arch. Ration. Mech. Anal.*, 98(2):123–142, 1987.

[67] L. Modica and S. Mortola. Un esempio di Γ-convergenza. *Boll. Unione Mat. Ital.*, 5(14-B):285–299, 1977.

[68] E. J. Nyström. Über die Praktische Auflösung von Linearen Integralgleichungen mit Anwendungen auf Randwertaufgaben der Potentialtheorie. *Commentat. Phys.-Math.*, 4(15):1–52, 1928.

[69] A. M. Oberman and J. Calder. Lipschitz regularized deep neural networks converge and generalize. `https://arxiv.org/abs/1808.09540`, 2018.

[70] J. A. Sethian. A fast marching level set method for monotonically advancing fronts. *Proc. Natl. Acad. Sci. USA*, 93(4):1591–1595, 1996.

[71] Z. Shi, B. Wang, and S. J. Osher. Error estimation of weighted nonlocal Laplacian on random point cloud. `https://arxiv.org/abs/1809.08622`, 2018.

[72] L. Simon. Lectures on geometric measure theory. In *Proceedings of the Centre for Mathematical Analysis, Australian National University*, volume 3. Australian National University Centre for Mathematical Analysis, 1983.

[73] M. I. Skolnik. *Radar handbook*. McGraw-Hill Book Co., 1970.

[74] D. Slepčev and M. Thorpe. Analysis of p-Laplacian regularization in semi-supervised learning. `https://arxiv.org/abs/1707.06213`, 2017.

[75] P. Strandmark, J. Ulen, F. Kahl, and L. Grady. Shortest Paths with Curvature and Torsion. In *2013 IEEE International Conference on Computer Vision(ICCV)*, pages 2024–2031. IEEE, 2013.

[76] C. Strode. Optimising multistatic sensor locations using path planning and game theory. In *IEEE Symposium on Computational Intelligence for Security and Defence Applications*, pages 9–16. IEEE, 2011.

[77] J. E. Taylor. Anisotropic interface motion. In *Mathematics of Microstructure Evolution*, volume 4 of *Empmd Monograph Series*, pages 135–148. The Minerals, Metals & Materials Society, 1996.

[78] M. Thorpe and F. Theil. Asymptotic Analysis of the Ginzburg–Landau Functional on Point Clouds. *Proc. R. Soc. Edinb., Sect. A, Math.*, 149:387–427, 2019.

[79] M. Thorpe and Y. van Gennip. Deep Limits of Residual Neural Networks. `https://arxiv.org/abs/1810.11741`, 2018.

[80] F. Tudisco and M. Hein. A nodal domain theorem and a higher-order Cheeger inequality for the graph p-Laplacian. *J. Spectr. Theory*, 8(3):883–908, 2018.

[81] Y. van Gennip. An MBO scheme for minimizing the graph Ohta–Kawasaki functional. *J. Nonlinear Sci.*, pages 1–49, 2018.

[82] Y. van Gennip and A. L. Bertozzi. Γ-convergence of graph Ginzburg–Landau functionals. *Adv. Differ. Equ.*, 17(11/12):1115–1180, 2012.

[83] Y. van Gennip, N. Guillen, B. Osting, and A. L. Bertozzi. Mean Curvature, Threshold Dynamics, and Phase Field Theory on Finite Graphs. *Milan J. Math.*, 82(1):3–65, 2014.

[84] U. von Luxburg. A tutorial on spectral clustering. *Statistics and Computing*, 17(4):395–416, 2007.

[85] D. Wagner and F. Wagner. Between min cut and graph bisection. In *International Symposium on Mathematical Foundations of Computer Science*, pages 744–750. Springer, 1993.